Si-rich 6*H*- and 4*H*-SiC(0001) 3×3 surface oxidation and initial SiO_2/SiC interface formation from 25 to 650 °C

F. Amy and P. Soukiassian
Commissariat à l'Energie Atomique, DSM-DRECAM-SPCSI-SIMA, Bâtiment 462, Saclay, 91191 Gif sur Yvette Cedex, France and Département de Physique, Université de Paris-Sud, 91405 Orsay Cedex, France

Y. K. Hwu
Academia Sinica, Nankang, Taipei, Taiwan

C. Brylinski
THALES, Laboratoire Central de Recherches, Domaine de Corbeville, B.P. 10, 91401 Orsay Cedex, France
(Received 13 November 2001; published 8 April 2002)

We investigate the initial oxidation of the Si-rich 6*H*-SiC(0001) 3×3 and 4*H*-SiC(0001) 3×3 surfaces and the subsequent SiO_2/4*H*-SiC and SiO_2/6*H*-SiC initial interface formation by Si *2p*, C *1s*, and O *1s* core-level photoemission spectroscopy using synchrotron radiation. The 3×3 surface reconstruction is found to be highly reactive to oxygen with an initial oxidation rate of about three to four orders of magnitude larger than for silicon surfaces. Furthermore, for both polytypes, direct SiO_2/SiC interface formation is achieved already at room temperature and extremely low oxygen exposures. However, the two polytypes have significantly different behaviors with larger amounts of oxide products having higher oxidation states for the 6*H*-SiC(0001) 3×3 surface, while mixed oxides including carbon species (Si-O-C) are the dominant oxide products for the *4H* polytype surface. The oxidation rate is improved at increased surface temperatures. In all cases, the oxygen uptake remains significantly larger for the *6H* polytype when compared to the *4H* one. The very different behavior of the *6H* and *4H* polytypes seems to originate, at least in part, from the presence of two domains in the bulk for the *4H* polytype (as evidenced by two bulk components in the Si *2p* core-level spectrum) which limits the oxygen insertion into the 4*H*-SiC lattice. Instead the *6H* polytype has only one bulk domain with a single Si *2p* bulk component. Abrupt SiO_2/6*H*-SiC interfaces could be achieved by thermal oxidation of a predeposited Si overlayer onto the surface leading to have oxide thicknesses ranging from 10 Å up to 80 Å after postoxidation with a transition layer of less than 5 Å. This study shows that, using a ''gentle'' initial oxidation approach at low temperatures and low oxygen exposures allow high-quality SiO_2/SiC interfaces. It also brings interesting insights into the understanding of polytype crucial effect in SiC surface oxidation.

DOI: 10.1103/PhysRevB.65.165323 PACS number(s): 81.65.Mq, 82.65.+r, 68.35.-p

I. INTRODUCTION

Silicon carbide (SiC) is certainly not a new material since it is older than the solar system. SiC has indeed been discovered more than a century ago (in 1895) by Henry Moissan on a meteorite fallen in the Diablo Canyon in Arizona.[1] But it is definitively an advanced material which has been initially known as ''carborundum'' for its excellent mechanical properties.[2] SiC is a IV-IV compound material belonging to the wide band-gap class of semiconductors. SiC exists in various crystallographic phases with more than 170 polytypes different by the stacking sequence periodicity and including cubic (β), rhombohedric and hexagonal (α) ones, with alternating Si and C atomic planes giving polar surfaces.[3,4] In addition to its strong fundamental interest, SiC is an advanced electronic material especially suitable for high-temperature, high-power, high-voltage, and high-frequency electronic devices and sensors.[2–7] Furthermore, SiC is one of the best biocompatible material.[8] It is only rather recently that well-defined SiC surfaces understood at the atomic scale could be obtained.[9–25] This has opened up the possibility of investigating the effect of adsorbate species such as molecules or metals on SiC surfaces and the corresponding interface formation.[26–32] Despite a higher carrier mobility for the cubic β-SiC, the hexagonal *6H*- and 4*H*-SiC phases are presently performed for potential applications primarily because of the availability of much better quality single-crystal wafers but also because of wider band gaps ranging from 3 eV (6*H*) to 3.3 eV (4*H*) instead of 2.4 eV for the cubic 3*C*-SiC.[2,3]

Surface passivation is one of the central issues in successful SiC device technology.[33,34] It is also of strong fundamental interest since, e.g., oxidation is among the most interesting elementary processes on surfaces. The success of silicon in microelectronics is in part due to the excellent properties of its native oxide (SiO_2) and to the low defect density of the SiO_2/Si interface. In these views, SiC is of special interest since its native oxide is also SiO_2.[33,34] Indeed, the SiO_2/SiC interface that forms during high-temperature oxidation allows field-effect transistor (FET) operation.[35] However, channel mobility in depletion mode FET are significantly lower than what could be expected considering bulk SiC properties and consequently a lot of studies have been devoted to SiO_2/SiC interface in order to improve channel mobilities. It appears that SiO_2/SiC interface has generally poor

electrical properties: due to the presence of carbon, conventional oxidation generally results in mixed oxide products including carbon and rough interfaces with high density of fixed charges and interface trap states.[3–5,36–39] Fixed charges are related to oxygen vacancies in the oxide,[37] while interface states are due to carbon atoms located at the interface.[36,37] Also of special interest is the fact that the interface state density for SiO_2/SiC interfaces has been shown to be significantly higher for the *4H* polytype (3.3 eV band gap) than for the *6H* one (2.9 eV band gap), likely located in the band gap below the conduction-band minimum. This leads to rather poor electrical properties, which is rather puzzling since both *6H* and *4H* polytypes have the same surface reconstruction.[3,4,18] Furthermore, despite higher bulk carrier mobilities for the 4*H*-SiC than for the 6*H*-SiC polytype, the *n*-channel mobilities for inversion 4*H*-SiC metal-oxide-semiconductor field-effect transistor is lower than for the 6*H*-SiC based ones.[40] Incidentally, this stresses the importance of having well-defined SiC surfaces in order to be in the position to achieve good quality SiO_2/SiC interfaces. Interface properties can be improved by postannealing in NO atmosphere.[41,42] The other approach is to start the interface formation from an atomically controlled reconstructed SiC surface and to use lower temperatures and lower oxygen exposure processes to initiate a ''gentle'' oxidation which could minimize surface/interface degradation during the oxidation process. SiC oxidation has recently been investigated by various experimental electrical and spectroscopic techniques using different approaches such as oxygen chemisorption, plasma-assisted oxidation, thermal oxidation, or catalytic oxidation ranging from the atomic scale initial oxidation to oxide/SiC interface formation.[26–28,30–32,36–39,41,43–45] However, these investigations are primarily focusing on the electrical and electronic properties with most of them studying nonwell-defined surfaces, and generally bringing little information if any on the oxide products and on the oxidation states at the interface, and on the interface structure. We have recently performed an atomic scale investigation of oxygen interaction onto the *6H*- and 4*H*-SiC(0001) 3×3 surface using scanning tunneling microscopy, core-level photoemission spectroscopy, and infrared absorption spectroscopy performed in the very low oxygen exposure regime ($\leqslant 1$ L$=1$ Langmuir, with 1 L$=10^{-6}$ Torr sec.).[45] Our results indicate the very high reactivity of the 6*H*- and 4*H*-SiC(0001) 3×3 surfaces especially when compared to silicon surfaces.[45] The oxygen molecule is readily dissociated at room temperature on the *6H*- and 4*H*-SiC(0001) 3×3 surfaces with no oxygen-atom interaction with the top surface atomic layer.[45] The oxygen atoms are found to bond to the Si adlayer located well below the surface, near the C atomic plane.[45]

In this paper, we present a comprehensive investigation of the initial oxidation of the Si-rich 6*H*- and 4*H*-SiC(0001) 3×3 surfaces and the subsequent SiO_2/SiC interface formation by core-level photoemission spectroscopy using synchrotron radiation for surface temperature ranging from 25 to 650 °C at oxygen exposures between 1 and 3000 L. Our results indicate the high reactivity to oxygen of the 3×3 surface reconstruction with oxide product formation at very low oxygen exposures, unlike the behavior of silicon surfaces. In addition, we find significant differences between the two polytypes with larger amounts of oxide products having higher oxidation states for the 6*H*-SiC(0001) 3×3 surface when compared to the 4*H*-SiC(0001) 3×3 one. The presence of mixed oxides including carbon species is found to be significantly more important for the *4H* polytype surface. In both cases, increasing the surface temperatures improves the efficiency of the oxidation process with larger oxidation products and higher oxidation states including SiO_2 formation with, once again, a more favorable situation for the *6H* polytype. The corresponding SiO_2/SiC interfaces are not abrupt with significant amounts of substoichiometric oxidation states including (Si^{3+}, Si^{2+}, and Si^{+}) and also mixed Si-O-C oxides products, SiO_2 being the dominant oxide product for the 6*H*-SiC(0001) 3×3 surface while substoichiometric oxides are predominant for the 4*H*-SiC(0001) 3×3 surface. In all cases, i.e., at room and higher temperatures, the oxygen uptake remains significantly larger for the *6H* polytype when compared to the *4H* one. Oxidation of a predeposited Si overlayer on the 6*H*-SiC(0001) 3×3 surface results in abrupt SiO_2/SiC interface formation with oxide thicknesses ranging from $\approx$10 to 80 Å and a transition layer having substoichiometric oxides of about $\leqslant$5 Å. The presence of two domains (in the bulk) for the *4H* polytypes which is evidenced by two bulk components in corresponding the Si *2p* core-level spectrum (unlike the *6H* which has only one bulk component) suggests a barrier to oxygen migration likely relevant in the observed different behavior to oxidation.

II. EXPERIMENTAL DETAILS

The photoemission spectroscopy experiments are performed at the Synchrotron Radiation Research Center (SRRC, Hsinchu, Taiwan). The light emitted by the third generation 1.5 GeV storage ring is dispersed by the high-energy spherical grating monochromator beam line. The photoelectron energy is analyzed using a hemispherical angle integrating ($\pm15°$ solid angle) electrostatic analyzer having a 150 mm radius. The overall (monochromator and analyzer) energy resolutions are 180 meV at the Si *2p*, 360 meV at the C *1s*, and 450 meV at the O *1s* core levels. The pressure in the vacuum chamber remains always in the mid 10^{-17} Torr range. We use 6*H*-*SiC*(0001) sample (Epitronics) *n*-type (between 7.10^{+17} and 8.10^{+18} cm^{-3} nitrogen doped) with a surface disoriented by 2.5° and 4*H*-SiC(0001) sample (Cree) *n*-type ($2.5.10^{+18}$ cm^{-3} nitrogen doped) with a surface disoriented by 3.5°. The *6H*- and 4*H*-SiC(0001) 3×3 surface preparation includes as the first step, an annealing at elevated temperatures ($\approx$1150 °C) in order to remove the native oxides and amorphous carbon or graphite. This process leads to a significant Si depletion from the surface, so the original as-received surface is totally removed for both *6H* and *4H* samples. In order to restore the Si stoichiometry, a 10 min Si deposition at 650 °C onto the surface is performed, followed by a 2 min annealing at 750 °C. Such a protocol results in smooth surfaces having very low defect densities—less than 2% of atomic defects—as checked by atom resolved scanning tunneling microscopy. In this way

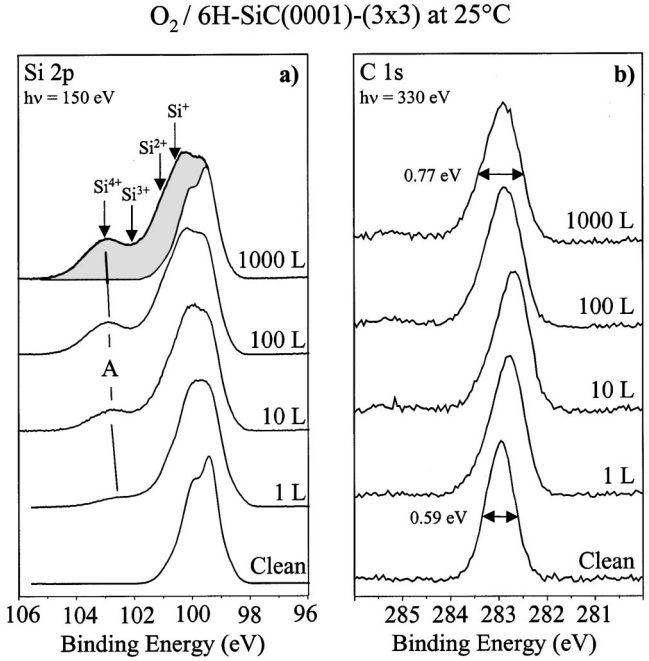

FIG. 1. (a) Si *2p* core level for the 6*H*-SiC(0001) 3×3 clean surface and exposed at 1 to 1000 L O_2 at 25 °C, recorded in the surface sensitive mode ($h\nu=150$ eV and emission angle $\theta_e=30°$). The chemically shifted component is labeled A while the Si^{4+}, Si^{3+}, Si^{2+}, and Si^{+} arrows indicate the binding energy of the four oxidation states of silicon. For the 1000 L O_2 exposure, the gray shaded area indicates the difference between spectra from the oxidized and the clean surface. (b) C *1s* core level for the clean 6*H*-SiC(0001) 3×3 surface and for the same oxygen exposure sequence as in (a) recorded in the surface sensitive mode ($h\nu=330$ eV and emission angle $\theta_e=30°$). C *1s* core-level peaks have full width at half maximum (FWHM) of 0.59 and 0.77 eV for the clean and 1000 L O_2 exposed surface, respectively.

and despite the sample different origins, the same morphology with high quality 3×3 surface reconstruction could be achieved for both *6H*- and 4*H*-SiC(0001) polytypes, making possible a comparison between them upon oxidation. Oxygen is deposited onto the surface using research grade oxygen exposures. The surface quality is checked by low-energy electron diffraction to have sharp 3×3 patterns. Additional details about high quality *6H*- and 4*H*-SiC(0001) 3×3 surface preparation could be found elsewhere.[19,30,45,46]

III. RESULTS

A. Oxidation of the 6*H*-SiC(0001) 3×3 surface at room temperature

We first look at the initial oxidation process at room temperature for the 6*H*-SiC(0001) 3×3 surface by exploring the formation of oxidation products at silicon and carbon sites using the Si *2p* and C *1s* core levels. Figure 1(a) displays the Si *2p* core level recorded at a 150 eV photon energy and grazing emission incidence (surface sensitive mode) for the clean and oxygen-exposed (from 1 to 1000 L) 6*H*-SiC(0001) 3×3 surface. Upon an O_2 exposure of 1 L, the Si *2p* core level exhibits a chemical shifted component A located at ≈102.8 eV binding energy. Peak A intensity increases at higher oxygen exposures ranging from 10 to 1000 L of O_2, with a higher binding energy at 103 eV, the latter value corresponding to silicon dioxide formation.[28,30,32,47,48] However, one can also notice that significant amounts of lower oxidation states are also present at 1000 L indicating a nonabrupt insulator/SiC interface formation.

Additional insights about oxygen interactions with the 6*H*-SiC(0001) 3×3 surface could be found by looking at the carbon atom environment using the C *1s* core-level line. Figure 1(b) displays the C *1s* for the same oxygen exposure sequence as in Fig. 1(a). First, one can notice that, unlike the Si *2p* core level, oxygen exposures do not result in a chemical shifted component at the C *1s* core level. Of principal interest, one can notice that the C *1s* core level is shifted to lower binding energy for increasing oxygen exposures, up to 0.3 eV at 10 L of O_2, and shifted back at its initial energy position for the clean surface at 1000 L of O_2. In addition, we also note a significant broadening of the C *1s* core level upon oxygen exposures by ≈30% at 1000 L for the full width at half maximum (FWHM) when compared to the value for the clean surface. Such a behavior indicates a certain degree of involvement of the C atoms in the oxidation products. Up to 10 L of O_2, the binding-energy decrease of the C *1s* indicates a change in the electronic status of C atoms resulting from O atoms interaction with Si atoms located close from the C atom plane.[45] The back shift to higher binding energy of the C *1s* core level about 10 L together with the large broadening (30% at 1000 L of O_2) suggest direct O atoms bonding to C atoms, most likely as a carbonatelike oxidation product such as Si-O-C.[28,30]

B. Oxidation of the 4*H*-SiC(0001) 3×3 surface at room temperature

We now turn to the initial oxidation of the 4*H*-SiC(0001) 3×3 surface at room temperature by looking at an oxygen exposure sequence ranging from 1 to 1000 L as for the 6*H*-SiC(0001) 3×3 surface described above. The oxidation sequence could be followed by looking at the set of Si *2p* core-level spectra in Fig. 2(a). A chemical shifted component slightly appears at the 102.8 eV binding energy for oxygen exposures above 10 L, i.e., at least ten times higher than for the 6*H*-SiC(0001) 3×3 surface. At 1000 L O_2 exposure, the oxide core-level shifted component A has its binding energy again reduces at 102.5 eV with apparently large amounts of substoichiometric oxide products when compared to the 6*H*-SiC(0001) 3×3 surface. Together with a necessary oxygen exposure ten times larger for the oxidation onset, this behavior indicates that the oxidation process is apparently much less efficient on the *4H* surface than on the *6H* one. Information about the interaction between oxygen and carbon atoms could be found by looking at the C *1s* core-level spectra for the same oxidation sequence as in Fig. 2(b). Interestingly, upon low oxygen exposures, we basically do not observe a C *1s* core-level shift to the lower binding energies as for the 6*H*-SiC(0001) 3×3 surface, but a 0.3 eV core-level shift to higher binding energy at 1000 L O_2 exposure. In addition, a very large broadening of the C *1s* core-level FWHM (by 60%) is taking place at the 1000 L O_2 exposure, i.e., two times larger than for the *6H* polytype. Such a be-

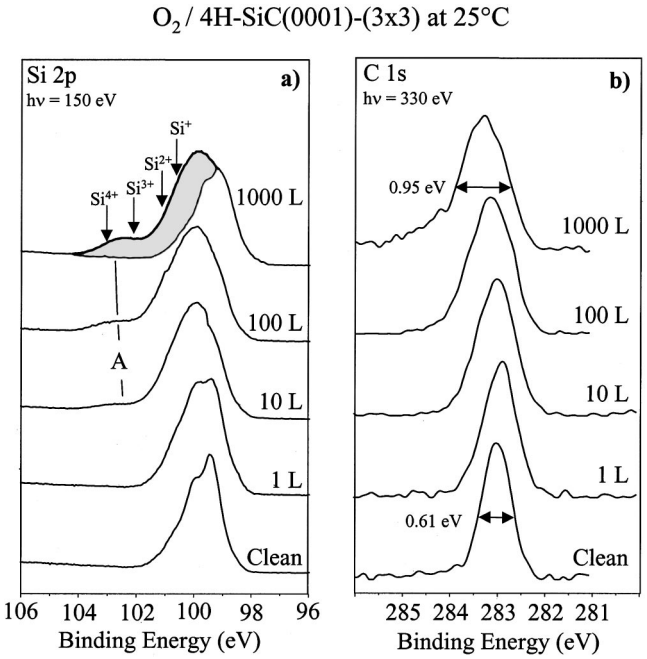

FIG. 2. (a) Si *2p* core level for the 4*H*-SiC(0001) 3×3 clean surface and exposed at 1 to 1000 L O_2 at 25 °C, recorded in the surface sensitive mode ($h\nu$=150 eV and emission angle θ_e =30°). The chemically shifted component is labeled A while the Si^{4+}, Si^{3+}, Si^{2+}, and Si^{+} arrows indicate the binding energy of the four oxidation states of silicon. For the 1000 L O_2 exposure, the gray shaded area indicates the difference between spectra from the oxidized and the clean surface. (b) C *1s* core level for the 4*H*-SiC(0001) 3×3 for the same sequence as in (a) recorded in the surface sensitive mode ($h\nu$=330 eV and emission angle θ_e =30°). C *1s* core-level peaks have full width at half maximum (FWHM) of 0.61 and 0.95 eV for the clean and 1000 L O_2 exposed surface, respectively.

havior suggests that, in contrast to the 6*H*-SiC(0001) 3×3 surface, the carbon atoms are immediately involved at the lowest oxygen exposures in the oxidation process, which is further supported by the formation of smaller amounts of silicon oxidation products which have lower oxidation states. Therefore, this stresses the formation of larger amounts of Si-O-C mixed oxides and carbonates products than for the 6*H*-SiC(0001) 3×3 surface which takes place already at the beginning step of the oxidation process.

C. Comparison between 6*H*- and 4*H*-SiC(0001) 3×3 surface oxidation at room temperature

To better stress the above differences in the oxidation regime between the 6*H*-SiC and 4*H*-SiC polytypes, we now look in Fig. 3 at a comparison between Si *2p* core levels for 1000 L O_2 exposures of both *6H*- and 4*H*-SiC(0001) 3×3 surfaces using relative binding-energy scale having its origin at 99.2 eV, i.e., the Si *2p* binding energy for pure silicon. Figure 3(a) displays the corresponding Si *2p* core level in the surface sensitive mode (emission angle 30° off the surface at a photon energy of $h\nu$=150 eV) and Fig. 3(b) in the bulk sensitive mode (emission angle 60° off the surface at a photon energy of $h\nu$=300 eV). One can better see from Fig.

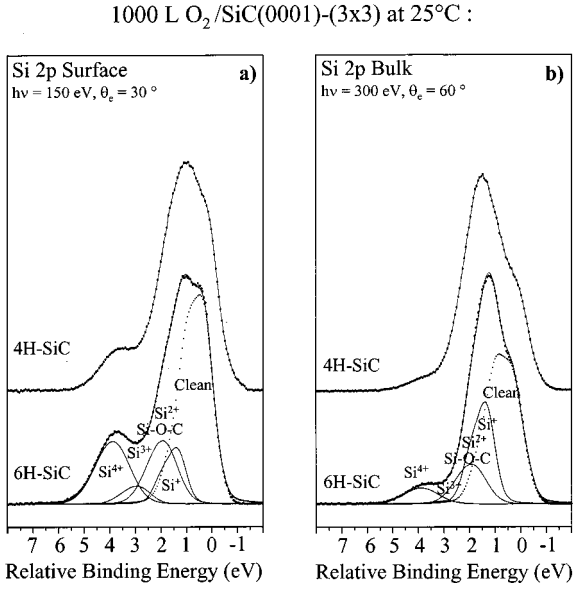

FIG. 3. Comparison between the Si *2p* core-level spectra for the 4*H*-SiC(0001) 3×3 and the 6*H*-SiC(0001) 3×3 surfaces exposed to 1000 L O_2 at 25 °C recorded in (a) surface sensitive mode ($h\nu$ =150 eV and emission angle θ_e=30°) and (b) bulk sensitive mode ($h\nu$=300 eV and emission angle θ_e=60°). The peak decomposition for the 1000 L of O_2/6*H*-SiC(0001) 3×3 surface show the silicon four oxidation states Si^{4+}, Si^{3+}, Si^{2+}, and Si^{+} (straight line). For the sake of clarity, the Si *2p* contribution of the clean SiC surface is represented by a single peak (dot line) that includes the two surface-shifted components (SS1 and SS2) and one bulk component B—see Fig. 4. The origin of the binding-energy scale is relative to the 99.2 eV corresponding to the Si *2p* binding energy for pure silicon.

3(a) that the amount of Si oxide products on the *6H* surface is significantly larger with higher oxidation states than for the corresponding 4*H*-SiC(0001) 3×3 surface, with, e.g., a higher binding energy of peak A for the *6H* surface. Figure 3(b) (bulk sensitive mode) displays a comparison for the bulk sensitive mode indicating the same trend. This behavior could be correlated to the much larger broadening observed at the C *1s* core level for the *4H* polytype when compared to the *6H* one which indicates a larger amount of mixed oxide products formation in the case of the 4*H*-SiC(0001) 3×3 surface.

To get deeper insights into the knowledge of oxidation states, we have performed a peak decomposition for the 1000 L of O_2/6*H*-SiC(0001) 3×3 surface [Figs. 3(a) and 3(b)]. For the sake of clarity, the Si *2p* contribution of the clean SiC surface is represented by a single peak that includes the two surface-shifted components (SS1 and SS2) and one bulk component B—see Fig. 4 below.[19,45] Notice that, in the very low oxygen exposure regime, the Si *2p* surface-shifted components (SS1 and SS2) are unaffected by oxygen atoms who have initial adsorption sites well below the surface.[45] The results exhibit four oxidation states corresponding to Si^{4+}, Si^{3+}, Si^{2+}, and Si^{+}, with Si^{4+} and Si^{2+} being the dominant features in the surface sensitive mode.[30] The situation looks rather similar in the bulk sensitive mode with however, some significant differences: the Si^{+} related peak is the only domi-

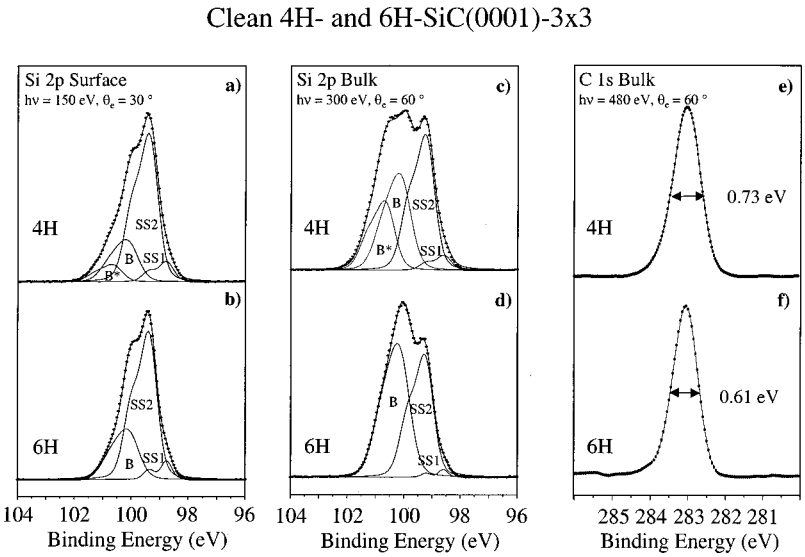

FIG. 4. Si *2p* core levels for clean 4*H*-SiC(0001) 3×3 and 6*H*-SiC(0001) 3×3 surfaces: (a) for clean 4*H*-SiC(0001) 3×3 and (b) clean 6*H*-SiC(0001) 3×3 recorded in the surface sensitive mode ($h\nu = 150$ eV and emission angle $\theta_e = 30°$); (c) for clean 4*H*-SiC(0001) 3×3, and (d) for clean 6*H*-SiC(0001) 3×3 recorded in the bulk sensitive mode ($h\nu = 300$ eV and emission angle $\theta_e = 60°$); (e) peak decomposition shows two surfaces shifted components SS1 and SS2 and one B (6*H*) or two B and B* (4*H*) bulk components; (f) C *1s* core levels for clean 4*H*-SiC(0001) 3×3, and (g) for clean 6*H*-SiC(0001) 3×3 recorded in the bulk sensitive mode ($h\nu = 480$ eV and emission angle $\theta_e = 60°$).

nant feature while Si^{3+} is basically absent. Notice that the lack of Si^{3+} and Si^{2+} oxidation states has been observed in the case of 4*H*-SiC(0001) $\sqrt{3}\times\sqrt{3}$ R30° surface, using very high oxygen exposures ($\approx 10^{+6}$ L of O_2) and high surface temperature (>800 °C), with however, the use of decomposition parameters that are apparently different.[32] The relatively large intensity for the Si^{2+} component together with the large broadening of the C *1s* core level clearly suggest a significant involvement of the C atoms in the oxidation process leading to mixed oxide products (Si-O-C) formation.[30]

Unfortunately, we are not able to successfully perform a similar peak decomposition for the 4*H*-SiC(0001) 3×3 oxidized surface using the same standards. We do, however, perform a Si *2p* core-level peak decomposition for the clean 4*H*-SiC(0001) 3×3 surface which is provided in Fig. 4, together with the corresponding curve fitting for the 6*H*-SiC(0001) 3×3 surface.[19] While the surfaces of both polytypes exhibit the same SS1 and SS2 surface-shifted and bulk B components, the 4*H*-SiC(0001) 3×3 surface surprisingly also displays a second bulk component labeled B* and located at 0.5 eV higher binding energy. This very different behavior is most likely related to the stacking sequence of the 4*H*-SiC polytype when compared to the 6*H*-SiC one. Indeed, while the latter has been shown to have almost a totally single domain stacking sequence (T3), the former instead exhibits clearly two domains (65% of T3 and 35% of T2).[48] This explains why the 4*H*-SiC(0001) 3×3 surface has an additional B* bulk component at the Si *2p* core level with the same B bulk component for both *4H*- and 6*H*-SiC(0001) 3×3 surface. Actually, it is interesting to correlate the different behavior observed at the Si *2p* core level for *6H* and *4H* to the corresponding C *1s* core level. Indeed, the C *1s* also shows some difference between the two polytypes with a linewidth that is 20% larger for the 4*H*-SiC(0001) 3×3 surface when compared to the 6*H*-SiC(0001) 3×3 surface [Figs. 4(e) and 4(f)]. In this view, it is unfortunately rather difficult to perform a reliable Si *2p* core-level peak decomposition evidencing the various silicon oxidation states of the 4*H*-SiC(0001) 3×3 surface.

Additional information about the room-temperature oxidation process could be found by looking in Fig. 5 at the O *1s* core level for both 6*H*- and 4*H*-SiC(0001) 3×3 surface at the same oxygen exposure sequence as in Figs. 1 and 2. As can be seen in Fig. 5(a) for the 6*H*-SiC(0001) 3×3 surface, the O *1s* basically includes three spectral features labeled *O* at ≈553.4 eV BE, *M* at ≈532 eV BE, and *N* at ≈530.7 eV BE. Peak *O* corresponds to the silicon dioxide formation in agreement with the picture seen above from the Si *2p* core level [Fig. 1(a)].[50] Peak *N* corresponds to carbonate mixed oxide products formation again in agreement with the above Si *2p* results [Fig. 1(a)].[50] Peak *M* appears to be the dominant spectral feature with a lower binding energy compared to

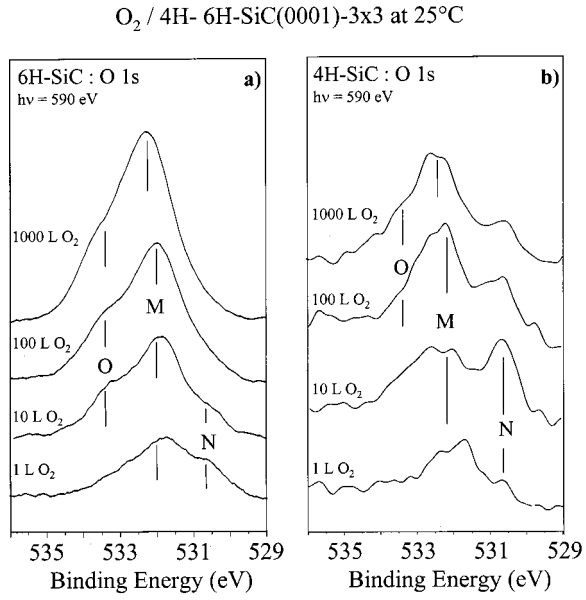

FIG. 5. O *1s* core-level spectra for (a) the 6*H*-SiC(0001) 3×3 and (b) 4*H*-SiC(0001) 3×3 surfaces exposed from 1 to 1000 L O_2 at 25 °C and recorded with a photon energy $h\nu = 590$ eV and an emission angle $\theta_e = 60°$. The three main peaks have been labeled O, M, and N and correspond to SiO_2, mixed plus suboxides and carbonate products formation, respectively.

peak *O* (SiO_2), therefore suggesting its assignment to the lower oxidation state oxide products. However, peak *M* is very wide and its contribution could also result from mixed oxide products including carbon species at a lower content compared to the carbonates. Interestingly, one can remark that the intensities of peaks *O* and *M* increase with the oxygen exposures while the intensity of peak *N* remains almost unaffected. This suggests that peak *M* is primarily due to substoichiometric Si oxides that are most probably located at the insulator/SiC interface.

Turning to the 4*H*-SiC(0001) 3×3 surface in Fig. 5(b), we basically notice the same three spectral features *O*, *M*, and *N* as for the 6*H*-SiC(0001) 3×3 surface, with however some significant differences regarding the relative intensities of each of these components. Of particular interest is the carbonate related peak *N* which is the dominant feature at low oxygen exposures (10 L) while the SiO_2 related peak *O* appears to be weak, therefore stressing once again that the oxidation process is less efficient for the *4H* polytype, in agreement with the picture derived above from the Si *2p* core level [Figs. 1(a) and 2(a)]. In addition, the behavior of peak *N* for the 4*H*-SiC(0001) 3×3 surface is consistent with C *1s* core levels broader (up to 25%) when compared to the 6*H*-SiC(0001) 3×3 surface indicating a more important C atom involvement in the oxidation products for the *4H* polytype.

D. Effect of temperature on the 6*H*- and 4*H*-SiC(0001) 3×3 surface oxidation

The effect of temperature on the 6*H*-SiC(0001) 3×3 surface oxidation process could be followed by looking at the Si *2p* core levels provided in Fig. 6. Figure 6(a) displays a representative set of Si *2p* core-level spectra recorded at various surface temperatures during an oxygen exposure of 1000 L, in the surface sensitive mode with a photon energy of $h\nu = 150$ eV. As can be seen from Fig. 6(a), upon increasing surface temperatures, the amount of oxidation products is dramatically increased especially favoring the high oxidation states (SiO_2). At 500 °C, the dominant oxide product appears to be siO_2 (Si^{4+}) with however, significant amount of lower oxidation states (Si^{3+}, Si^{2+}, Si^{+}, and also Si-O-C mixed oxides) clearly indicating a nonabrupt SiO_2/6*H*-SiC interface formation.[28,30,43] In order to probe the oxide formation in the subsurface and bulk regions, we record the Si *2p* core level in a bulk sensitive mode for the same sequence as in Fig. 6(a) using a photon energy of 300 eV at a photoelectron emission angle of 60°. Figure 6(b) shows the corresponding sequence which stresses even better the nonabrupt character of the SiO_2/6*H*-SiC interface with the dominant spectral feature located at 100.9 eV BE, corresponding to Si^{2+} oxidation state and probably also to Si-O-C mixed oxide formation,[28,30,42] with much smaller amounts of Si^{4+} (SiO_2) present below the surface. Again, one can clearly see that higher temperatures result in a dramatic increase of the amount of oxide products.

We now compare the oxidation behavior of the 6*H*-SiC(0001) 3×3 surface with the 4*H*-SiC(0001) 3×3 one. Figure 7(a) exhibits Si *2p* core levels in the surface sensitive mode for the 6*H*-SiC(0001) 3×3 and

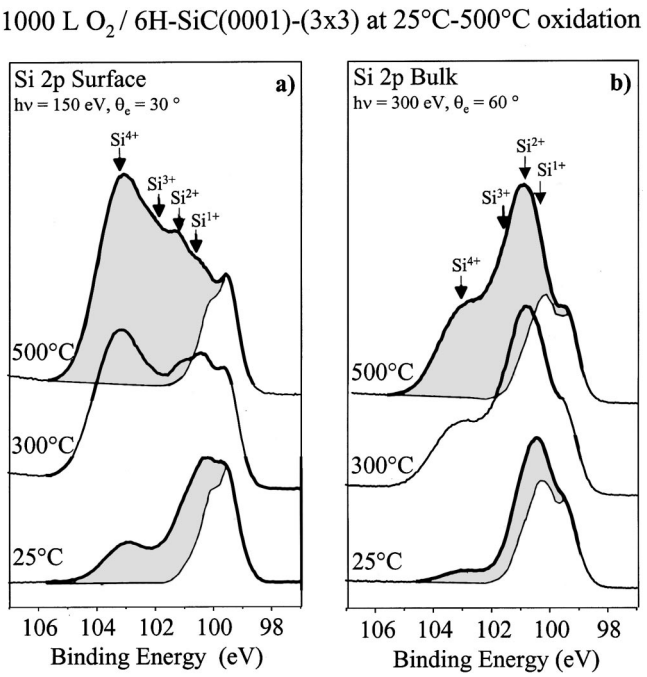

FIG. 6. Si *2p* core-level spectra for the 6*H*-SiC(0001) 3×3 surface exposed at 1000 L O_2 for different substrate temperatures ranging from 25 to 500 °C and recorded (a) in the surface sensitive mode ($h\nu = 150$ eV and emission angle $\theta_e = 30°$) and (b) in the bulk sensitive mode ($h\nu = 300$ eV and emission angle $\theta_e = 60°$). The Si^{4+}, Si^{3+}, Si^{2+}, and Si^{+} arrows indicate the binding energy of the four oxidation states of silicon and the gray shaded area indicates the difference between spectra from the oxidized and the clean surfaces.

4*H*-SiC(0001) 3×3 surface exposed to 1000 L of O_2 at 500 °C while Fig. 7(b) shows the same sequence of oxidation in the bulk sensitive mode. As can be seen by a simple visual inspection, one can immediately note dramatic differences between the two polytypes, that are much more pronounced than the ones observed in Figs. 1 and 2 for the room-temperature oxidation sequences. In the surface sensitive mode [Fig. 7(a)], the dominant spectral feature for the *4H* polytype is located at 2.7 eV binding energy while for the *6H* polytype, the most intense peak is located at 4.5 eV relative binding energy. Peak decomposition for the latter indicates SiO_2 as the main oxide product while for the 4*H*-SiC(0001) 3×3 surface, intermediate oxidation states and mixed Si-O-C oxides are responsible for the dominant peak at 2.7 eV. Unfortunately, while we are able to achieve a peak decomposition for the *6H* surface, it is also not possible to do so for the *4H* one, because of the B* additional bulk component existing on 4*H*-SiC(0001) (see above in Fig. 4) which overlaps with the chemically shifted components resulting from the lowest oxidation states. Next, we explore the subsurface and bulk regions by looking in Fig. 7(b) at the differences between the two polytypes upon oxidation in the photoemission bulk sensitive mode. It is evident from Fig. 7(b) that the chemically shifted component related to intermediate and mixed oxides is much more intense for the *4H* by 85%. This behavior not only stresses that the oxide/SiC interface is not abrupt for both polytypes but also that the intermediate and mixed oxides are always dominant for the 4*H*-SiC(0001) surface.

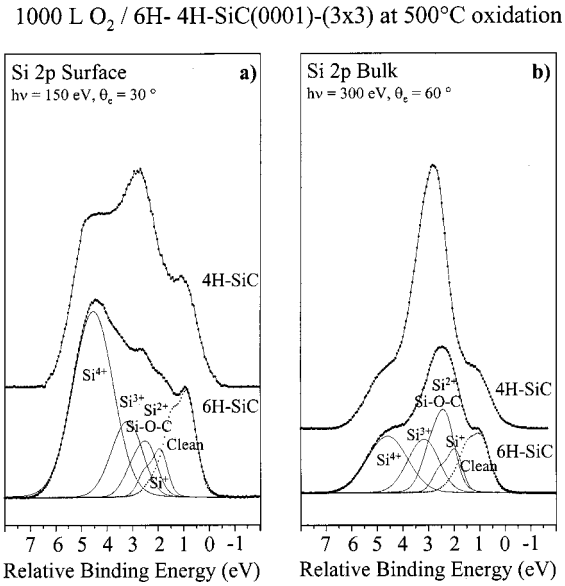

FIG. 7. Comparison between the Si *2p* core-level spectra for the 4*H*-SiC(0001) 3×3 and 6*H*-SiC(0001) 3×3 surfaces exposed to 1000 L O_2 at 500 °C in (a) surface sensitive mode ($h\nu=150$ eV and emission angle $\theta_e=30°$) and (b) bulk sensitive mode ($h\nu=300$ eV and emission angle $\theta_e=60°$). The peak decomposition for the 1000 L of O_2/6*H*-SiC(0001) 3×3 surface show the four oxidation products Si^{4+}, Si^{3+}, Si^{2+}, and Si^{+} (straight line). For the sake of clarity, the Si *2p* contribution of the clean SiC surface is represented by a single peak (dot line) that includes the two surface-shifted components (SS1 and SS2) and one (or two) bulk components B (B*)—see Fig. 4. The relative binding-energy scale is relative to the 99.2 eV binding energy of Si *2p* in pure silicon.

Additional insights about the *6H*- and 4*H*-SiC oxidation process at 500 °C could be found using the O *1s* core level at various oxygen exposures. Figure 8(a) displays the O *1s* core level for the 6*H*-SiC(0001) 3×3 surface exposed to O_2 (from 1 to 1000 L) at 500 °C. At a low oxygen exposure (1 L), the O *1s* exhibits two features *M* and *N* located at 532 eV and ≈530.6 eV corresponding to intermediate and mixed oxide products (*M*) and carbonate species (*N*), respectively. In contrast, the higher oxygen exposures result in a single O *1s* core-level component located at 533 eV and corresponding to SiO_2 formation which, in agreement with the above Si *2p* core level (Fig. 7), stresses that SiO_2 is the dominant oxidation product for the *6H* polytype. A totally different scenario is taking place for the corresponding *4H* polytype as can be seen in Fig. 8(b) with peak *N* related to carbonate products being the dominant feature at 10 and 100 L of O_2 exposures while peak *M* (intermediate oxidation states plus mixed oxide products) is the dominant one at a 1000 L of O_2 exposure.

In order to evaluate the oxygen uptake at various surface temperatures and different oxygen exposures, we plot in Fig. 9 the integrated intensity of the O *1s* core level for both *6H*- and 4*H*-SiC(0001) 3×3 surfaces. As can be seen in Fig. 9, the oxygen uptake for the *4H* polytype remains always below that of the *6H* polytype, regardless of the O_2 exposures and/or the surface temperature. Another interesting feature is

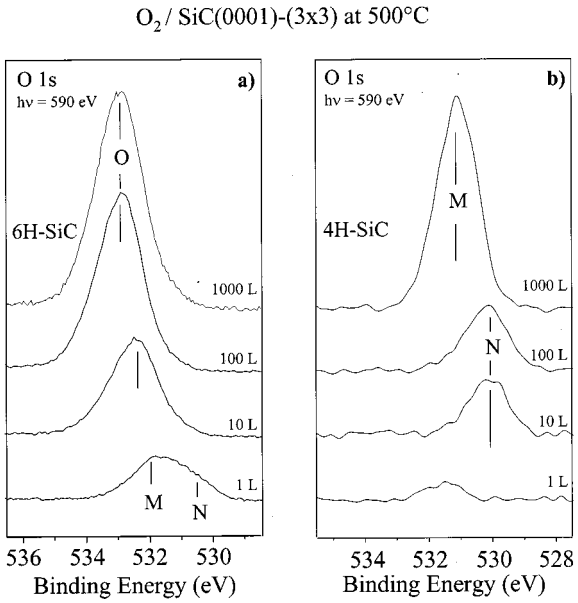

FIG. 8. O *1s* core-level spectra for the (a) 6*H*-SiC(0001) 3×3 and (b) 4*H*-SiC(0001) 3×3 surfaces exposed from 1 to 1000 L O_2 at 500 °C recorded with a photon energy $h\nu=590$ eV and an emission angle $\theta_e=60°$ (surface sensitive mode). The three main peaks have been labeled O, M, and N and correspond to SiO_2, mixed plus suboxides and carbonate products formation, respectively.

the effect of surface temperature which increases the oxygen uptake in the higher oxygen exposure regime for the *4H* and *6H* surfaces. In fact, increasing surface temperatures is likely to favor oxygen atom migration below the surface, which indeed is likely to become more efficient in the higher oxygen deposition regimes.

E. SiO_2/6*H*-SiC(0001) interface formation by predeposited Si overlayer oxidation

Since the direct oxidation of the Si-rich 3×3 surfaces of *6H*- and 4*H*-SiC(0001) always results in nonabrupt interfaces, it is interesting to explore alternative approaches such as the oxidation of a predeposited Si overlayer onto the surface. Figure 10 exhibits Si *2p* core levels recorded in the

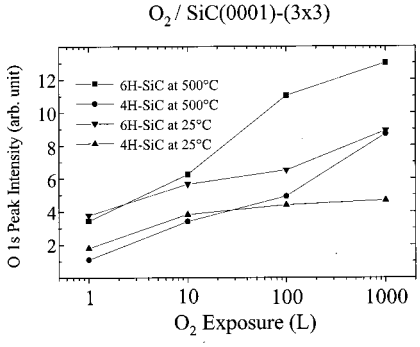

FIG. 9. Comparison of the oxygen uptake on the 4*H*-SiC(0001) 3×3 and 6*H*-SiC(0001) 3×3 surfaces at 25 and 500 °C. O *1s* peak intensity is displayed using arbitrary units and correspond to the integrated surface of the core-level peak.

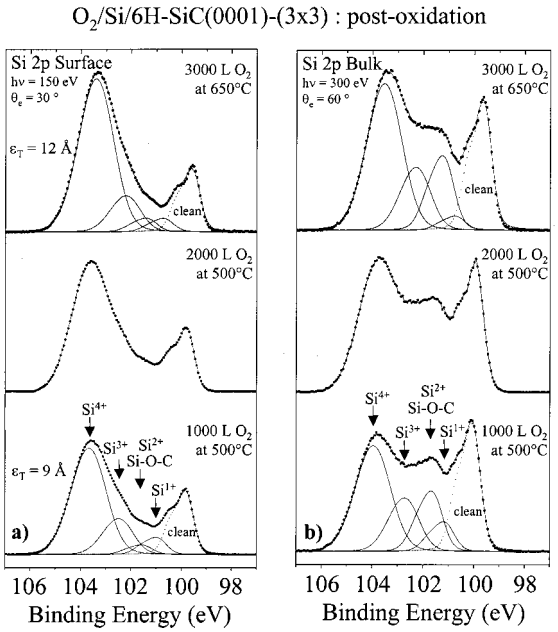

FIG. 10. Thermal oxidation of a predeposited Si overlayer onto the 6*H*-SiC(0001) 3×3 surface followed by a postoxidation sequence: Si *2p* core-level spectra for the Si/6*H*-SiC(0001) surface exposed to 1000 L O_2 at 500 °C and then reexposed to a total of 2000 L O_2 at 500 °C and 3000 L O_2 at 650 °C recorded in (a) surface sensitive mode ($h\nu=150$ eV and emission angle $\theta_e=30°$) and (b) bulk sensitive mode ($h\nu=300$ eV and emission angle $\theta_e=60°$). The total oxide thickness (ε_t) is 9 Å for the Si/6*H*-SiC(0001) and surface exposed to 1000 L O_2 at 500 °C and 12 Å for the 3000 L O_2 at 650 °C. The Si *2p* core-level peak decomposition for the O_2/Si/6*H*-SiC(0001) surface shows the four oxidation products Si^{4+}, Si^{3+}, Si^{2+}, and Si^{+} (straight line). For the sake of clarity, the Si *2p* contribution of the clean SiC surface is represented by a single peak (dot line).

surface and bulk sensitive modes for a Si overlayer deposited onto the 6*H*-SiC(0001) surface and exposed to 1000 and 2000 L of O_2 at 500 °C, and 3000 L at 650 °C. As can be seen from Fig. 10, the SiO_2/6*H*-SiC interfaces look much more abrupt than those obtained by direct SiC oxidation. In all cases, the dominant spectral feature is corresponding to SiO_2 oxide products. We perform peak decomposition for the 1000 L (500 °C) and 3000 L (650 °C) oxidation sequences in order to evaluate the relative importance of these various oxidation states. First, we note the presence of the silicon substoichiometric oxidation states (Si^{3+}, Si^{2+}, Si^{+}) with also Si-O-C mixed oxides.[28,30,43] However, the latter has been shown to be present only at the interface between the pure oxide and the SiC surface with oxygen atoms bonded to both C and S atoms.[28,30,43] In this way, the oxidation process probably always stops on a carbon atomic plane.[28,30,43] Notice that this Si overlayer has been shown to have an unexpected and novel cubic 4×3 array growing on hexagonal SiC surface and to be highly sensitive to oxygen, likely due to higher surface electronic densities favoring oxygen molecular dissociation.[51] This is very likely to be at the origin of rather abrupt SiO_2/6*H*-SiC interface formation.[30]

TABLE I. Oxides thickness deduced from peak decomposition and attenuation layer model. ε_t is the total oxide thickness including SiO_2, mixed and suboxides, ε_{SiO_2} is the SiO_2 thickness and ε_{sub} the thickness of the mixed and suboxides.

	1000 L O_2 at 500 °C	3000 L O_2 at 650 °C
Percentage of SiO_2 versus total amount of oxides	49%	55%
ε_T= Total oxides thickness	9 Å	12 Å
ε_{SiO_2}= SiO_2 thickness	4.5 Å	6.7 Å
ε_{sub}= Suboxides thickness	4.5 Å	5.3 Å

Next, using the photoelectron attenuation layer method,[47] we determine the total oxide thickness which is 9 Å at 1000 L and 500 °C at 12 Å at 3000 L and 650 °C. These values are consistent with ellipsometry spectroscopic measurements performed independently and also showing that oxygen exposures up to 120 000 L at 500 °C results in a total oxide thickness of about 80 Å.[52] From the oxide thickness and the integrated intensities of the Si *2p* chemically shifted components (in the bulk sensitive regime), it is possible to extract the respective thicknesses of the silicon dioxide and of the substoichiometric oxidation products. The results are provided in Table I. This gives thicknesses of 4.5 Å for both SiO_2 and substoichiometric oxides at an oxygen exposure of 1000 L at 500 °C, and 6.7 Å for SiO_2 products and 5.3 Å at an oxygen exposure of 3000 L at 650 °C. This indicates a transition oxide layer that is about a few atomic layers thick ($\approx<3$ atomic layers) which is rather thin. On such SiO_2/6*H*-SiC interfaces, it is potentially possible to grow thicker silicon dioxide without interface degradation.

IV. DISCUSSION

Our above results support a picture of *6H*- and 4*H*-SiC(0001) 3×3 surface reconstructions which is extremely reactive to oxygen since the growth of oxide products is already detected at very low oxygen exposures (≈1 L) and at room temperature. This behavior is in sharp contrast to the case of silicon for which oxide growth is taking place at oxygen exposures higher by several orders of magnitude (3 to 4).[47,48,53] While this high surface reactivity of the 3×3 reconstruction applies to both *6H* and *4H* polytypes, one should remark that the former one is even much more reactive than the latter. Indeed, the room-temperature oxidation of the 6*H*-SiC(0001) 3×3 surface results in larger amounts of silicon oxides having higher oxidation states than for the corresponding 4*H*-SiC(0001) 3×3 surface. In both cases, the oxide/SiC interfaces are not abrupt with significant amounts of intermediate oxidation states (Si^{3+}, Si^{2+}, and Si^{+}) but also mixed oxide species containing carbon atoms as Si-O-C, the latter being more present for the 4*H*-SiC(0001) 3×3 surface. One of the striking differences between the *6H*- and the 4*H*-SiC(0001) 3×3 surface is the presence of two bulk components for the latter one. This feature could be related to the presence for the 4*H*-SiC of two domains in the bulk corresponding to different building

blocks bulk termination in the stacking sequence as recently observed experimentally.[49] Therefore, one can easily imagine that block boundaries could act as a limiting factor in oxygen interactions, diffusion, and finally insertion into the SiC lattice, thereby resulting in a lower oxidation rate for the *4H* polytype.[49] Together with other features such as large differences in the electronic properties, this factor is likely to play an important role in limiting the oxidation rate of the 4*H*-SiC(0001) 3×3 surface and in the formation of oxide products having properties significantly degraded (especially for the oxide/SiC interface) when compared to the situation occurring for the 6*H*-SiC(0001) 3×3 surface.

When the surface temperature is increased, we have seen above that the amount of oxidation products increases significantly for both *6H*- and 4*H*-SiC(0001) 3×3 surfaces with however, the same significant differences in the oxidation products and interface quality. The major oxidation product at 500 °C is SiO_2 for the *6H* polytype, while mixed and substoichiometric oxides are the dominant ones for the *4H* surface indicating that, despite higher temperatures favoring oxygen subsurface penetration, the oxygen migration and subsequently insertion into the lattice seems to be significantly lower for the *4H* polytype. Indeed, when looking at the oxygen uptake at various exposures, and at room temperature and 500 °C (Fig. 9), one can clearly see that the oxygen uptake for the *4H* remains always below the oxygen uptake for the *6H* polytype, regardless of the surface temperature. This probably stresses the fact that structural differences between both polytypes remain the key limiting factor in the 4*H*-SiC(0001) 3×3 surface oxidation, even at elevated temperatures. Furthermore, the O *1s* (Fig. 8) as well as the Si *2p* (Fig. 7) core levels show the much higher involvement of the carbon atoms with larger amounts of mixed Si-O-C oxides. However, it is interesting to notice that the oxide thicknesses are about the same for both polytypes, despite that the 6*H*-SiC(0001) 3×3 surface exhibits higher oxidation states with primarily SiO_2 as the dominant oxide product.

Turning to the SiO_2/6*H*-SiC interface formation by oxidation of a predeposited Si overlayer, we have seen above that it is possible to achieve abrupt SiO_2/6*H*-SiC interfaces with basically very little if any carbon atom involvement into the oxidation products. Together with our previous study,[30] our finding is in sharp contrast to the conclusions drawn in recent theoretical *ab initio* calculations probing the Si-O bonding configurations and predicting that, contrary to the case of SiO_2/Si interfaces, an abrupt SiO_2/SiC interface cannot be achieved.[54] Our results clearly show that this is not the case, thereby stressing that one has to be very careful when making predictions based on calculations not taking into consideration the entropy and performed for a system ''frozen'' at 0 K. Indeed, the abrupt SiO_2/SiC interface is obtained after high-temperature annealings which involve delicate kinetics and complex effects that are not taken into consideration in the calculations of Ref. 54. Such ''static'' calculations, which are performed on laterally limited atomic models, cannot address the complex dynamical processes that are occurring here during the oxide/substrate interface formation and safely derive information about the latter. In addition, these calculations are neither SiC polytype specific, nor SiC surface reconstruction specific[54] which, as reported previously[28,30,43] and also observed here are definitely of central importance in SiO_2/SiC interface formation, quality, and composition.

Actually, the structure of the predeposited Si thin film (few atomic layers) which has been shown to organize into a novel and unexpected cubic 4×3 structure seems to be here of crucial importance in the successful abrupt interface formation.[51] Indeed, such a structure has a very open array most probably favoring oxygen atom migration into the bulk.[51] In addition, the 4×3 cubic Si thin film has been shown to have a higher electronic-filled states density which would favor oxygen molecule dissociation.[51] The other very interesting feature is the formation of a carbon-free SiO_2/6*H*-SiC interface at 500 °C. It is likely that upon high temperatures, the oxygen atoms are also oxidizing the carbon layer. Such a process would result in CO or CO_2 species that are desorbed into the vacuum upon elevated temperature annealings (≈500 °C) and in subsequent abrupt SiO_2/6*H*-SiC interface formation. Such a mechanism has indeed been found to occur for alkali-metal promoted oxidation of cubic 3*C*-SiC oxidation as evidenced experimentally by x-ray photoemission spectroscopy.[27] A similar mechanism of oxidized C atom desorption as CO or CO_2 molecular species should also take place and would be favored at elevated temperatures for the direct oxidation of the 6*H*-SiC(0001) 3×3 and 4*H*-SiC(0001) 3×3 surfaces. However, the mechanism that limits oxygen diffusion and insertion in the 4*H*-SiC lattice is likely to also interfere with CO and CO_2 emission, thus leading to a more carbon-rich SiO_2/SiC interface on the *4H* polytype when compared to 6*H*-SiC one as indeed found here. Overall, the above results suggest that the oxygen atoms passing through the Si overlayer are more active, possibly as negative O^{--} ions. Indeed, the role of such negative oxygen ion species has been suggested for alkali-metal promoted oxidation of semiconductor surfaces. For the Si covered 6*H*-SiC(0001) surface, the results also suggest that the oxidation process stops at a C plane, leading to have at the interface, oxygen atoms bonded to both C and Si atoms. This would be responsible for the remaining Si *2p* small chemical shifted component located around 101.7 eV BE [Fig. 10(a)].

Finally, it is interesting to remark that the postoxidation at 650 °C does not destroy the SiO_2/6*H*-SiC interface with a thicker oxide layer reaching 12 instead of 9 Å in the case of the initial oxidation at 500 °C. The transition layer between SiO_2 and the 6*H*-SiC surface includes few atomic layers of substoichiometric oxides (≈3) having a thickness of about ≈5 Å. This interesting finding would allow one to use such a system to regrow additional oxide thereby permitting a thicker SiO_2 overlayer while still keeping an abrupt interface. One should also keep in mind that these SiO_2/6*H*-SiC interfaces are grown here at rather low temperatures (when compared to conventional oxidation processes used in device technology in which temperatures around 1000 °C are commonly used), which probably minimizes C atoms' involvement in the oxidation process and results in abrupt interface formation. Also, a low-temperature process provides oxides that are known to be more resistant to the radiation damages.

V. CONCLUSIONS

Using synchrotron radiation based core-level photoemission spectroscopy, we have investigated in detail the initial oxidation of the Si-rich *6H*- and 4*H*-SiC(0001) 3×3 surfaces and the subsequent SiO_2/SiC interface formation at various surface temperatures (25–650 °C) and low O_2 exposures from 1 to 3000 L. The 3×3 surface reconstruction is found to be highly reactive to oxygen with oxidation rates three to four orders of magnitude larger than for silicon surfaces and, unlike silicon, oxide product formation at already extremely low oxygen exposures (<1 L O_2) and room temperature. The behavior of the two polytypes is found to be significantly different with larger amounts of oxide products having higher oxidation states for the 6*H*-SiC(0001) 3×3 surface, and presence of mixed oxides including carbon species that are significantly more important for the *4H* polytype surface. Increasing the surface temperature improves the oxidation rate with larger amounts of oxide products having higher oxidation states primarily consisting of SiO_2 formation for the *6H* polytype while the *4H* polytype, the 3×3 surface mostly exhibits substoichiometric (Si^{3+}, Si^{2+}, and Si^{+}) and *C* containing mixed (Si-O-C) oxide formation. Whatever the surface temperature is, the oxygen uptake remains significantly larger for the *6H* polytype when compared to the *4H* one. The very different behavior of the *6H* and *4H* polytypes is likely to originate, at least in part, from the presence of two domains in the bulk for the *4H* polytype as evidenced by the two bulk components in the Si *2p* core-level spectrum (unlike the *6H* which has only one bulk component). Such a structural difference probably limits oxygen atom insertion into the *4H*-SiC lattice. When a predeposited Si overlayer on the 6*H*-SiC(0001) 3×3 surface is exposed to oxygen at elevated temperatures (500–650 °C), an abrupt SiO_2/SiC interface formation is achieved with oxide thicknesses ranging from $\approx$10 to 80 Å and a transition layer having substoichiometric oxides of about $\approx$5 Å. The very open 4×3 cubic structure of the Si overlayer together with the possible existence of negative oxygen ion species are most likely the key factors in carbon-free and abrupt SiO_2/6*H*-SiC interface formation. It is also interesting to remark that using a ''gentle'' oxidation approach including low-temperature processing (<650 °C when compared to the much higher temperatures generally used, e.g., in device technology) and low oxygen exposures allows the growth of high-quality SiO_2/SiC interfaces. These findings, which also stress the crucial role of SiC polytypism, bring insights into the understanding of silicon carbide oxidation.

ACKNOWLEDGMENTS

This work was supported in part by the Institut Français de Taipei (IFT), by the National Science Council (NSC, Taipei), and by the Délégation Générale à l'Armemant (DGA, Paris, France). It is based upon research conducted at the Synchrotron Radiation Research Center (SRRC), Hsinchu, Taiwan. The authors are especially grateful to the SRRC staff for expert and outstanding assistance and to Dr. Tseng for the use of his experimental system, and to Alfred Hofrichter and Bernard Drevillon at Ecole Polytechnique, Palaiseau, France, for performing state-of-the-art spectrometric ellipsometry measurements of the oxide thickness on the SiC surfaces.

[1] H. Moissan, Acad. Sci., Paris, C. R. **139**, 773 (1904).

[2] F. Bozso, L. Muehlhoff, M. Trenary, W. J. Choyke, and J. T. Yates, Jr., J. Vac. Sci. Technol. A **2**, 1271 (1984); J. Bouix, M. P. Berthet, F. Bosselet, R. Favre, M. Peronnet, J. C. Viala, C. Vincent, and H. Vincent, J. Phys. IV **7**, 191 (1997), and references therein.

[3] *Silicon Carbode, A Review of Fundamental Questions and Applications to Current Device Technology*, Vols I & II, edited by W. J. Choyke, H. M. Matsunami, and G. Pensl (Akademic Verlag, Berlin, 1998), and references therein.

[4] *Properties of Silicon Carbide*, edited by G. Harris, EMIS Datareview Series, Vol. 13 (INSPEC, London, 1995), and references therein.

[5] Mater. Res. Bull. **22**, XX (1997).

[6] IEEE Trans. Electron Devices **46** (March) (1999), and references therein.

[7] V. M. Aroutiounian, V. V. Bouniatian, and P. Soukiassian, Solid-State Electron. **43**, 343 (1999).

[8] J. C. Bokros, R. J. Akins, H. S. Shim, A. D. Hanbold, and N. K. Agarwal, Chem. Technol. **7**, 40 (1977); K. L. Smith and K. M. Black, J. Vac. Sci. Technol. A **2**, 744 (1984).

[9] V. M. Bermudez, Phys. Status Solidi B **202**, 447 (1997), and references therein.

[10] P. Soukiassian and F. Semond, J. Phys. IV **7**, 10 (1997), and references therein.

[11] P. Soukiassian, Mater. Sci. Eng., B **61**, 506 (1999), and references therein.

[12] F. Semond, P. Soukiassian, A. Mayne, G. Dujardin, L. Douillard, and C. Jaussaud, Phys. Rev. Lett. **77**, 2013 (1996).

[13] P. Soukiassian, F. Semond, L. Douillard, A. Mayne, G. Dujardin, L. Pizzagalli, and C. Joachim, Phys. Rev. Lett. **78**, 907 (1997).

[14] P. Soukiassian, F. Semond, A. Mayne, and G. Dujardin, Phys. Rev. Lett. **79**, 2498 (1997).

[15] V. Derycke, P. Soukiassian, A. Mayne, G. Dujardin, and J. Gautier, Phys. Rev. Lett. **81**, 5868 (1998); V. Derycke, P. Soukiassian, A. Mayne, and G. Dujardin, Surf. Sci. Lett. **446**, L101 (2000).

[16] H. W. Yeom, M. Shimomura, J. Kitamura, S. Hara, K. Tono, I. Matsuda, B. S. Mun, W. A. R. Huff, S. Kono, T. Ohta, S. Yoshida, H. Okuski, K. Kajimura, and C. S. Fadley, Phys. Rev. Lett. **83**, 1640 (1999).

[17] K. Reuter, J. Bernhardt, H. Wedler, J. Schardt, U. Starke, and K. Heinz, Phys. Rev. Lett. **79**, 4818 (1997).

[18] U. Starke, J. Schardt, J. Bernhardt, M. Franke, K. Reuter, H. Wedler, K. Heinz, J. Furthmuller, P. Kackell, and F. Bechstedt, Phys. Rev. Lett. **80**, 758 (1998).

[19] F. Amy, P. Soukiassian, Y. K. Hwu, and C. Brylinski, Surf. Sci. Lett. **464**, L691 (2000).
[20] J. Schardt, J. Bernhardt, U. Starke, and K. Heinz, Phys. Rev. B **62**, 10 335 (2000).
[21] A. Coati, M. Sauvage-Simkin, Y. Garreau, R. Pinchaux, T. Argunova, and K. Aïad, Phys. Rev. B **59**, 12 224 (1999).
[22] L. I. Johansson, F. Owman, and P. Martensson, Phys. Rev. B **53**, 13 793 (1996).
[23] I. Forbeaux, J. M. Themlin, and J. M. Debever, Phys. Rev. B **58**, 16 396 (1998).
[24] M. Naitoh, J. Takami, S. Nishigaki, and T. Toyama, Appl. Phys. Lett. **75**, 650 (1999).
[25] M. A. Kulakov, G. Henn, and B. Bullemer, Surf. Sci. **346**, 49 (1996).
[26] V. M. Bermudez, Appl. Surf. Sci. **84**, 45 (1995).
[27] M. Riehl-Chudoba, P. Soukiassian, C. Jaussaud, and S. Dupont, Phys. Rev. B **51**, 14 300 (1995).
[28] F. Semond, L. Douillard, P. Soukiassian, D. Dunham, F. Amy, and S. Rivillon, Appl. Phys. Lett. **68**, 2144 (1996).
[29] F. Semond, P. Soukiassian, P. S. Mangat, Z. Hurych, L. di Cioccio, and C. Jaussaud, Appl. Surf. Sci. **104**, 79 (1996).
[30] F. Amy, P. Soukiassian, Y. K. Hwu, and C. Brylinski, Appl. Phys. Lett. **75**, 3360 (1999).
[31] L. Simon, L. Kubler, A. Ermolieff, and T. Billon, Phys. Rev. B **60**, 5673 (1999).
[32] C. Virojanadara and L. I. Johansson, Surf. Sci. Lett. **472**, L145 (2001).
[33] S. M. Sze, *Modern Semiconductor Devices Physics* (Wiley-Interscience, New York, 1998).
[34] *Fundamental Aspects of Ultrathin Dielectrics on Si-based Devices*, edited by E. Garfunkel, E. Gusev, and A. Vul', Vol. 3 of *NATO Science Series High Technology* (Kluwer Academic, Dortrecht, 1998).
[35] L. A. Lipkin and J. W. Palmour, J. Electron. Mater. **25**, 909 (1996); and references therein.
[36] V. R. Vathulya, D. N. Wang, and M. H. White, Appl. Phys. Lett. **73**, 2161 (1998); V. V. Afanas'ev, A. Stesmans, M. Bassler, G. Pensl, M. J. Schulz, and C. I. Harris, *ibid.* **68**, 2141 (1996).
[37] V. V. Afanas'ev and A. Stesmans, Appl. Phys. Lett. **69**, 2252 (1996); V. V. Afanas'ev, A. Stesmans, M. Bassler, G. Pensl, M. J. Schulz, and C. I. Harris, J. Appl. Phys. **85**, 8292 (1999).
[38] J. N. Shenoy, J. A. Cooper, Jr., and M. R. Melloch, Appl. Phys. Lett. **68**, 803 (1996); W. Xie, J. N. Shenoy, S. T. Sheppard, M. R. Melloch, and J. A. Cooper, Jr., *ibid.* **68**, 2231 (1996).
[39] B. Hornetz, H.-J. Michel, and J. Halbritter, J. Vac. Sci. Technol. A **13**, 767 (1995); C. Önneby and C. G. Pantano, *ibid.* **15**, 1597 (1997).
[40] R. Schorner, P. Friedrichs, D. Peters, and D. Stephani, IEEE Electron Device Lett. **20**, 241 (1999).
[41] H. F. Li, S. Dimitrijev, H. B. Harrison, and D. Sweatman, Appl. Phys. Lett. **70**, 2028 (1997).
[42] G. Y. Chung, C. C. Tin, J. R. Williams, K. McDonald, M. Di Ventra, S. T. Pantelides, L. C. Feldman, and R. A. Weller, Appl. Phys. Lett. **76**, 1713 (2000).
[43] P. Soukiassian, in *Fundamental Aspects of Ultrathin Dielectrics on Si-based Devices*, edited by E. Garfunkel, E. Gusev, and A. Vul', Vol. 3 of *NATO Sciences Series High Technology* (Kluwer Academic, Dortrecht, 1998), p. 257.
[44] G. Lucovsky and H. Niimi, in *Fundamental Aspects of Ultrathin Dielectrics on Si-based Devices*, edited by E. Garfunkel, E. Gusev, and A. Vul', Vol. 3 of *NATO Science Series High Technology* (Kluwer Academic, Dortrecht, 1998), p. 447.
[45] F. Amy, H. Enriquez, P. Soukiassian, P. F. Storino, Y. J. Chabal, A. J. Mayne, G. Dujardin, Y. K. Hwu, and C. Brylinski, Phys. Rev. Lett. **86**, 4342 (2001).
[46] C. Radtke, I. J. R. Baumvol, J. Morais, and F. C. Stedile, Appl. Phys. Lett. **78**, 3601 (2001).
[47] F. J. Himpsel, F. R. McFeely, A. Taleb-Ibrahimi, J. A. Yarmoff, and G. Hollinger, Phys. Rev. B **38**, 6084 (1988); and references therein.
[48] Z. H. Lu, M. J. Graham, S. P. Tay, D. T. Jiang, and K. H. Tan, J. Vac. Sci. Technol. B **13**, 1626 (1995); and references therein.
[49] U. Starke, J. Schardt, and M. Franke, Appl. Phys. A: Mater. Sci. Process. **65**, 587 (1997); J. Schardt, J. Bernhardt, U. Starke, and K. Heinz, Surf. Rev. Lett. **5**, 181 (1998); U. Starke, J. Schardt, J. Bernhardt, M. Franke, and K. Heinz, Phys. Rev. Lett. **82**, 2107 (1999).
[50] O. Kubaschewski, C. D. Alcock, and P. J. Spencer, in *Materials Thermochemistry*, 6th ed. (Pergamon, Oxford, 1993).
[51] F. Amy, H. Enriquez, P. Soukiassian, C. Brylinski, A. Mayne, and G. Dujardin, Appl. Phys. Lett. **79**, 767 (2001).
[52] A. Hofrichter, B. Drevillon, F. Amy, and P. Soukiassian (unpublished).
[53] M. Tabe, T. T. Chiang, I. Lindau, and W. E. Spicer, Phys. Rev. B **34**, 2706 (1986).
[54] R. Buczko, S. J. Pennycook, and S. Pantalides, Phys. Rev. Lett. **84**, 943 (2000).